Journal of Medicinal Chemistry

Article

Important Hydrogen Bond Networks in Indoleamine 2,3-dioxygenase 1 (IDO1) Inhibitor Design revealed by Crystal Structures of Imidazoleisoindole Derivatives with IDO1

Yi-Hui Peng, Shau-Hua Ueng, Chen-Tso Tseng, Ming-Shiu Hung, Jen-Shin Song, Jian-Sung Wu, Fang-Yu Liao, Yu-Shiou Fan, Mine-Hsine Wu, Wen-Chi Hsiao, Ching-Cheng Hsueh, Shu-Yu Lin, Chia-Yi Cheng, Chih-Hsiang Tu, Lung-Chun Lee, Ming-Fu Cheng, Kak-Shan Shia, Chuan Shih, and suying wu

J. Med. Chem., **Just Accepted Manuscript** • DOI: 10.1021/acs.jmedchem.5b01390 • Publication Date (Web): 07 Dec 2015

Just Accepted

ACS Publications

Journal of Medicinal Chemistry is published by the American Chemical Society. 1155 Sixteenth Street N.W., Washington, DC 20036

Important Hydrogen Bond Networks in Indoleamine 2,3-dioxygenase 1 (IDO1) Inhibitor Design revealed by Crystal Structures of Imidazoleisoindole Derivatives with IDO1

Yi-Hui Peng,[†] Shau-Hua Ueng,[†] Chen-Tso Tseng,[†] Ming-Shiu Hung,[†] Jen-Shin Song,[†] Jian-Sung Wu,[†] Fang-Yu Liao,[†] Yu-Shiou Fan,[†] Mine-Hsine Wu,[†] Wen-Chi Hsiao,[†] Ching-Cheng Hsueh,[†] Shu-Yu Lin,[†] Chia-Yi Cheng,[†] Chih-Hsiang Tu,[†] Lung-Chun Lee,[†] Ming-Fu Cheng,[†] Kak-Shan Shia,[†] Chuan Shih,[†] Su Ying Wu.[†]*

[†] Institute of Biotechnology and Pharmaceutical Research, National Health Research Institutes, 35, Keyan Road, Zhunan Town, Miaoli County 350, Taiwan, ROC

KEYWORDS: Indoleamine 2,3-dioxygenase 1 (IDO1), imidazoleisoindole, NLG919, IDO1 inhibitors, hydrogen bond network, intramolecular hydrogen bond, structural biology

ABSTRACT

Indoleamine 2,3-dioxygenase 1 (IDO1), promoting immune escape of tumors, is a therapeutic target for the cancer immunotherapy. A number of IDO1 inhibitors have been identified but only limited structural biology studies of IDO1 inhibitors are available to provide insights on the binding mechanism of IDO1. In this study, we present the structure of IDO1 in complex with **24**, a NLG919 analogue with potent activity. The complex structure revealed the imidazole nitrogen atom of **24** to coordinate with the heme iron, and the imidazoleisoindole core situated in pocket A with the 1-cyclohexyl ethanol moiety extended to pocket B to interact with the surrounding residues. Most interestingly, **24** formed an extensive hydrogen bond network with IDO1, which is a distinct feature of IDO1/**24** complex structure and is not observed in the other IDO1 complex structures. Further structure-activity relationship, UV-spectra and structural biology studies of several analogues of **24** demonstrated that extensive hydrophobic interactions and the unique hydrogen bonding network contributes to the great potency of imidazoleisoindole derivatives. These results are expected to facilitate the structure-based drug design of new IDO inhibitors.

Introduction

Indoleamine 2,3-dioxygenase 1 (IDO1) is a heme-containing enzyme that catalyzes the initial and rate limiting step in the catabolism of tryptophan via the kynurenine pathway, leading to the formation of a series of biologically active metabolites, including the final product nicotinamide adenine dinucleotide (NAD).[1,2] It catalyzes the oxidative ring cleavage of various substrates, including tryptophan, 5-hydroxytryptophan, serotonin and tryptamine. Through the catabolism of tryptophan, IDO1 inhibits the proliferation and differentiation of T cells, which are sensitive to the degradation of tryptophan and accumulation of tryptophan catabolites.[3] IDO1 is found to be over-expressed in cancer cells, acting as a direct guard against T-cell attack, and is also expressed within antigen presenting cells to enhance peripheral tolerance to tumor associated antigens (TAAs) in tumor draining lymph nodes.[4] By these mechanisms, IDO1 facilitates the survival, growth, invasion, and metastasis of malignant cells expressing TAAs by protecting them from recognition and attack by the immune system. *In vivo* studies showed that IDO1 deficiency resulted in impaired tumor growth, metastases development delay, and prolonged survival in an $IDO1^{-/-}$ animal model, validating IDO1 as a therapeutic target for the cancer immunotherapy.[5]

Several IDO1 inhibitors have showed efficacy when used alone or in combination with other therapeutics, and are currently in the clinical trials. One of the most advanced, hydroxyamidine compound (INCB024360, also named epacadostat), developed by Incyte, is an orally bioavailable small molecule inhibitor of the IDO1 protein, with potent enzymatic and cellular activity.[6] It was also shown to enhance T lymphocyte, dendritic cell and natural killer cell responses *in vitro*. As in the *in vivo* study, INCB024360 was efficacious as a single agent or in combination use with cytotoxic and immunotherapy agents in cancer mouse models.[7] INCB024360 currently undergoes several clinical trials, either used as a monotherapy or in combination with various antibody, in subjects with advanced or metastatic cancers. Another IDO1 inhibitor, NLG919 (an imidazoleisoindole derivative; the chemical structure is undisclosed), developed by NewLink Genetics and later licensed to Genentech as GDC-0919, is undergoing phase I clinical trials in the treatment of recurrent advanced solid tumors.[8] NLG919 showed potent inhibition of IDO1 in both enzymatic and cellular assays. The *in vivo* study revealed that oral administration of NLG919 reduced the concentration of kynurenine in plasma and tissue by around 50%. Treatment with NLG919 showed dose-dependent activation and proliferation of effector T cells, and led to the dramatic regression of tumor size. The ability of NLG919 to reduce tumor growth was highly correlated with its functional immune

response, which is consistent with its proposed mechanism of action as an immune modulator. The dose repeat toxicity (NOAEL) of rat and dog were both at 80 mg/kg/day in 28 days, BID.[8] In addition, when combined with Indoximod, NLG919 showed synergistic T cell activation and tumor regression.[8] No dose limiting toxicities have been observed so-far, and the safety and toxicity of NLG919 in patients is currently being evaluated. In addition to INCB024360 and NLG919, various IDO inhibitors have been discovered by several pharma companies, and are now in the different stages of drug development.[9-13]

Although various IDO1 inhibitors with diverse chemical structures have been reported, only few crystal structures of IDO1 bound to inhibitors are available in the public domain.[14,15] The first is the structure of IDO1 in complex with 4-phenylimidazole (4-PI), a fragment-like ligand with weak inhibition against IDO1 (IC_{50} = 48 μM).[16,17] As revealed by ligand-bound structures, 4-PI was found to be located in the binding site (pocket A) with its phenyl ring inserting into a lipophilic cavity, and one nitrogen atom of the imidazole ring interacting to the heme iron.[14] In addition to pocket A, however, the binding site could extend to the adjacent hydrophobic pocket (pocket B), consisting of Phe163, Phe226, Arg231, Leu234 and Ile354 residues, which larger ligands might target. Whereas pocket A is the major binding site involving heme-binding, pocket B could be targeted to improve the binding affinity. Recently,

Tojo et al. reported two inhibitors co-crystallized with IDO1[15]: (2-(5-*p*-tolylthiazolo[2,3-*c*][1,2,4]triazol-3-ylthio)-*N*-(benzo[*d*][1,3]dioxol-5-yl)aceta mide) (IC_{50} = 3.0 μM);[10] and the imidazothiazole derivative **27** (IC_{50} = 1.9 μM).[15] These two compounds induced a conformation change in pocket A, resulting from the movement of main chain Ala260-Ser263 and the shift of Phe226 and Arg231, and extended into the pocket B. The structural information suggests that the interactions with Phe226 and Arg231 contribute to the increased potency of these imidazothiazole derivatives to IDO1.

As could be seen from the foregoing discussion, all the published IDO structures up-to-date are complexed with weak inhibitors with inhibition potency at micromolar range. Therefore, the structures of IDO in complex with potent inhibitors are needed to gain a better understanding of the binding mechanism of IDO1 and further provide molecular insights to design novel and potent inhibitors. In this study, we present the structure of IDO1 in complex with **24** at 2.2 Å. Compound **24,** a NLG919 analogue, contains an imidazoleisoindole core and exhibits potent inhibitory activity to IDO1 with the IC_{50} value of 38 nM. The crystal structure revealed **24** to occupy both pocket A and B, coordinating with the heme iron atom through the imidazole nitrogen and making hydrophobic interactions with the surrounding residues. Interestingly, **24** forms an extensive hydrogen bond network with IDO1; there are two intermolecular

hydrogen bonds between **24**, the 7- propionic acid group of the heme and the main chain NH group of Ala264; and an intramolecular hydrogen bond within **24** between the isoindole nitrogen and the hydroxyl group. This hydrogen bond network is a distinct feature of the IDO1/**24** complex structure and is not observed in the other IDO1 complex structures. Moreover, the detailed structure-activity relationship (SAR) information of NLG919 analogues, i.e. imidazoleisoindole derivative, are not disclosed[18] and UV-spectra studies of these analogues are unavailable. In this study, structure-activity relationship, UV-spectra, and several co-crystal structures of imidazoleisoindole derivatives are also presented to elucidate the inhibition mechanisms of this series of compounds.

Results and Discussion

Biological Activity of 24. Compound **24** (1-cyclohexyl-2-(5*H*-imidazo[5,1-*a*]isoindol-5-yl)ethanol)**,** a NLG919 analogue, was synthesized and evaluated by biological assays. Compound **24** contains two chiral centers; one adjacent to the cyclohexyl group, and the other at the 5-position of the imidazoleisoindole ring (Figure S1 in the supporting information). This results in four stereoisomers, designated as **28** ((R)-1-cyclohexyl-2-((S)-5*H*-imidazo[5,1-*a*]isoindol-5-yl)ethanol), **29** ((S)-1-cyclohexyl-2-((S)-5*H*-imidazo[5,1-*a*]isoindol-5-yl)ethanol), **30**

((S)-1-cyclohexyl-2-((R)-5*H*-imidazo[5,1-*a*]isoindol-5-yl)ethanol) and **31** ((R)-1-cyclohexyl-2-((R)-5*H*-imidazo[5,1-*a*]isoindol-5-yl)ethanol) (Figure S1). Compound **24**, a mixture of four stereoisomers (**28**, **29**, **30** and **31**), inhibited IDO1 with IC_{50} value of 38 nM.

A UV-visible spectra study[19] was performed to evaluate the binding of compound **24**. IDO1 is a heme-containing protein and the unique UV absorption properties of porphyrins are useful in studies of heme-proteins.[20,21] The absorbance spectra of the heme group is highly sensitive to the changes in the polarity of heme surroundings upon the ligand/substrate binding, which changes the spectral properties of the heme.[22] Therefore, the changes in the UV-visible spectra causing by the IDO1-ligand interaction could be utilized to evaluate the binding of compounds to IDO1. The UV-visible spectra of ferric IDO1 were measured in the presence and absence of compound **24** (Figure 1). In the absence of compound **24**, the absorption spectrum of ferric IDO1 exhibited a Soret peak at 403 nm, similar to the previous publications.[21] This shifted to 413 nm in the presence of compound **24**, demonstrating that compound **24** binds to IDO1 and coordinates with the iron of the heme group.

Structural Biology Studies of Compound 24. To further elucidate the binding mode and to gain insights into the detailed interactions of compound **24** with IDO1, human IDO1 protein was purified and co-crystallized with **24**. The IDO1/**24** co-crystals

formed in 1~2 weeks and were red in color. The structure of IDO1 in complex with compound **24** was solved to a resolution of 2.2 Å. The space group was found to be $P2_12_12_1$ with two IDO1 monomers in the asymmetric unit. The electron density maps of IDO1/**24** were clear, except for some disordered regions that included residues 360-380 in monomer A, and residues 361-375 in monomer B. The monomer of IDO1 consists of two domains: one is the large domain and the other is the small domain. The heme-binding pocket is located in the large domain and residue His346 was coordinated to the heme iron atom at the fifth coordination position. The electron density map clearly showed that **24** was located at the sixth coordination site of the heme, and covalently bound to the heme iron (Figure 2 and Figure S1). Since IDO1 was crystallized with a mixture of all four stereoisomers of **24**, all of these stereoisomers were built into the density map to investigate which isomers majorly bind to IDO1. The 2Fo-Fc and Fo-Fc map of all four stereoisomers were presented in Figure S1. A difference map, showing differences between the model and the experimental data, could detect the misplacement of the ligand[23,24] and also the wrong conformation or stereochemistry of the ligand.[25,26] Positive difference density were found near two chiral centers of **30** and **31**. In contrast, no positive difference density were observed around **28** and **29**, suggesting **28** and **29** fit properly in the density map. These two stereoisomers were therefore selected for further model building and

refinement. The results showed that both stereoisomers, **28** (R,S-stereoisomer) and **29** (S,S-stereoisomer), superimposed well with each other and made almost identical interactions with IDO1. Therefore, **28** (R,S-stereoisomer) and **29** (S,S-stereoisomer), both contribute to the inhibition of IDO1, which is consistent with the later biological analysis of **28** and **29** showing that they inhibited IDO1 with very similar IC_{50} values.

From the foregoing stereoisomer study, the R,S configuration of **24** is used for the discussion in the IDO1/**24** complex structure. **24** was found to coordinate with the heme iron through the imidazole nitrogen atom (Figure 2A). This direct binding of **24** with the heme iron is characterized as a type II interaction[27] and is supported by the UV-visible spectra data: **24** was found to induce a Soret band red shift from 403 to 413 nm upon the binding to heme iron. The imidazoleisoindole core is situated deep in pocket A and formed extensive hydrophobic interactions with Tyr126, Cys129, Val130, Phe163, Phe164, Gly262, Ala264 and the porphyrin ring. The 1-cyclohexyl ethanol moiety extended to pocket B and formed hydrophobic interactions with Phe226, Ile354 and Leu384, and also had close contacts with Arg231 in the entrance region (Figure 2A). Most interestingly, **24** formed an extensive hydrogen bond network with the heme group and the protein residues in the active site (Figure 2B). This hydrogen bond network consisted of a hydrogen bond formed by the hydroxyl group of **24** with the 7- propionic acid of the heme; a hydrogen bond formed by the

propionic acid side chain with the main chain NH group of Ala264; and an intramolecular hydrogen bond formed within **24** by the isoindole nitrogen and the hydroxyl group.

The IDO1/**24** complex structure suggests that some functional groups of **24** would contribute to the binding of **24** to IDO1 and thus affect the inhibitory potency. For example, the imidazoleisoindole group coordinated to the heme iron and formed hydrophobic interactions with residues in pocket A; the hydroxyl group was involved in the hydrogen bond network with IDO1; and the isoindole nitrogen participated in the intramolecular hydrogen bonding to stabilize **24** and the binding to IDO1. Preorganization of ligand by the intramolecular hydrogen bond would lead to decreased entropic cost of binding and consequently result in increased affinity.[28,29] To further investigate the contributions of these pharmacophores in the binding to and inhibition of IDO1, and advance structure-based drug design, several analogues of **24** were synthesized to explore structure-activity relationship (SAR), and structural biology studies performed to elucidate the detailed interactions between these analogues with IDO1 (Table 1).

Chemistry. Compound **22–26** were synthesized according to the procedures established by the Newlink Genetics Co[30] and the compound identification data of those was listed in the supporting information. The synthesis of

1-cyclohexyl-2-(3-methyl-5*H*-imidazo[5,1-*a*]isoindol-5-yl)ethanol (**8**) from 2-methylimidazole **1** followed the synthetic paths established by the Newlink Genetics Co.[30] and described in scheme 1.

Compound **15** was synthesized by the methods shown in scheme 2. β-Oxo-cyclohexanepropanal **10** was prepared by the condensation of cyclohexylethanone (**6**) and ethyl formate (**9**) following the literature reported procedure.[31] 4-(2-Aminophenyl)imidazole **13** was synthesized by a Suzuki coupling of iodoimidazole **11** and pinacol borate **12**, and then compound **13** was reacted with **10** to give tricyclic compound **14**. Reduction of the ketone group of compound **14** with sodium borohydride gave the resulted imidazo[1,5-*c*]quinazolinyl ethanol **15**.

Compounds **18**, **20**, and **21** were prepared using established methods with necessary modifications (scheme 3). *N*-Alkylation of norharmane (**16**) and 2-bromo-1-cyclohexylethan-1-one gave ketone **17**, which was reduced using sodium borohydride to give 2-*β*-carbolin-9-yl-1-cyclohexyl-ethanol **18**. The synthesis of compounds **20** and **21** followed the same procedure as mentioned above with α-carboline **19** as the starting material.

SAR Studies. When a fluoro group was introduced in the imidazoleisoindole to generate **25**, it showed 2-fold improvement in the inhibition to IDO1 compared to **24**. As shown in UV-visible spectra**, 25** induced the same red shift as **24**, from 403 nm to

413 nm**,** indicating **25** could also make the coordinated covalent bond with the heme iron. The replacement of the hydroxyl group with carbonyl group (**22**) resulted in a 12- fold decrease in inhibition of IDO1 as compared with **24**. Similarly, replacement of the hydroxyl group with carbonyl group (**23**) resulted in a 14-fold decrease in IDO1 inhibitory activity, compared to its hydroxyl analogue **25**. These results shows the important role played by the hydroxyl group in the inhibition to IDO1. The effect of a halogen group on the potency was also investigated: compound **23** with an additional fluorine group relative to compound **22** showed 2-fold higher potency than **22**. Further modifications of the imidazoleisoindole ring of **24** to give **8** and **26** led to a complete loss of activity toward IDO1. In **8**, the imidazole ring was replaced with the 2-methylimidazolyl ring and the activity decreased significantly. The reason for this dramatic loss of activity could be that the additional methyl group at the C2-position of the imidazole could result in a steric clash with the heme group in IDO1 and thus prevent the formation of the coordination covalent bond with the heme iron. This hypothesis is supported by the UV-visible spectra of **8**, which showed only a weak Soret signal from 403 to 405 nm, suggesting that **8** was unable to coordinate with heme iron. Compound **24**, in contrast, induced an obvious Soret signal, from 403 to 413 nm. Compound **26**, a triazolyl analogue formed by modification of the C-2 position of the imidazole ring of **24**, showed no IDO1 inhibitory activity, consistent

with a described study.[32] Modifications of the isoindole ring of **24** were also found to affect the binding to and inhibition of IDO1. Expansion of the 5-membered isoindole ring of **24** to a six-membered quinazoline ring generated **15**, resulting in a 29-fold decrease in IDO1 activity. A molecular docking study of **15** in the active site of IDO1 was performed and compared with the IDO1/**24** complex structure (Figure S2) to elucidate the difference in binding interactions between **15** and **24**. It was found that although the imidazole nitrogen formed the coordinate covalent bond with the heme iron as evidenced by its induced Soret red shift from 403 to 413 nm, the ring expansion of **15** rearranged the orientation of the 1-cyclohexyl ethanol moiety such that the hydroxyl group became located away from the quinazoline nitrogen (distance = 4.3 Å) and was therefore unable to form an intramolecular hydrogen bond within **15**.

Another structural modification, replacement of the five-membered imidazoleisoindole ring of **24** with a six-membered, 9*H*-pyrido[3,4-*b*]indole ring to generate **18**, resulted in almost complete loss of activity ($IC_{50} > 10$ μM). The UV-visible spectra revealed that **18** showed a smaller spectral change (403 to 407 nm) upon binding to IDO1 than that observed for **24**, indicating the weaker interactions of **18** with the heme group. A co-crystal structure of IDO1 with **18** revealed that the hydroxyl group of **18** was unable to form the hydrogen bond with the heme (Figure 4)

and the nitrogen atom in the pyridine ring was further away from the heme iron (see below section of Structure-based Drug Design of imidazoisoindole Compounds). Finally, the modification of imidazoleisoindole ring of **24** to a 9*H*-pyrido[2,3-*b*]indole, **20** or **21**, led to the complete loss of activity. **20** and **21** showed no inhibition against IDO1 and the UV-visible spectra of IDO1 in the presence of **21** (or **20**) was the same as that of the native IDO1 protein alone. These results suggest that **20** and **21** were unable to form the coordinated covalent bond with the heme iron, which may explain the complete loss of inhibitory activity.

Structure-Based Drug Design of imidazoisoindole Compounds. In order to elucidate the binding mode of imidazoisoindole derivatives at the molecular level, compounds **23**, **25**, and **18** were co-crystallized with the IDO1 protein and the structures were solved (Table S1). Superimposition of the structure of IDO1/**25** complex (Figure 3A) and that of the IDO1/**24** complex revealed (Figure 3C) these two compounds adopted very similar conformations in the active site, and formed similar coordinated covalent bond, hydrogen bond networks and hydrophobic interactions with the surrounding residues. The difference between these two inhibitors is the additional fluorine group to make an extra halogen bonding interaction with the oxygen atom in the main chain of Gly 262 in pocket A (Figure 3A), which contributes to the 2-fold improved potency of **25** as compared with **24**.

As revealed in the above mentioned SAR studies, the replacement of the hydroxyl group of **25** with a carbonyl group to give **23**, decreased the inhibitory potency 14-fold. The same trend was also observed for **22** and **24**. To investigate the role played by this hydroxyl group in the binding to the IDO1 protein, the structure of the IDO1/**23** complex (Figure 3B) was solved and compared with that of IDO1/**25** complex. The two structures superimposed well (Figure 3C) to each other and both coordinated with heme iron, and also formed extensive hydrophobic interactions and a halogen bond with the protein. However, in the IDO1/**23** complex structure, the carbonyl group was unable to serve as a hydrogen bond donor to allow the intramolecular hydrogen bond to the isoindole nitrogen. The loss of this intramolecular hydrogen bond could be the reason for the decrease in inhibitory activity of **23.** This comparison of IDO1/**23** and IDO1/**25** emphasizes the contribution of the intramolecular hydrogen bond on the inhibition of IDO1.

SAR studies found that replacement of the imidazoisoindole core of (**24**) with the 9*H*-pyrido[3,4-*b*]indole core to give **18** led to a dramatic loss of IDO1 inhibitory activity and also resulted in a smaller UV-vis shift (403 to 407 nm). To understand these changes, **18** was co-crystallized with IDO1 and the structure was solved (Figure 4A and Table S1). The hydroxyl group of **18** was found to be moved away from the propionic acid with distance > 4.3Å, with loss of the intermolecular hydrogen bond

with the heme (Figure 4). In comparison, the hydroxyl group of **24** was shifted toward the propionic acid group where it formed a strong intermolecular hydrogen bond with the heme. In addition, the 9*H*-pyrido[3,4-*b*]indole core was found to be shifted away from the heme, a distance of 2.44Å separating the pyridine nitrogen and the heme iron. In comparison, the imidazoisoindole core of **24** is closer to the heme iron. The absence of the hydrogen bonding interactions with the heme group in IDO1 and the weaker coordinate covalent interactions would provide the explanations for the shorter UV-vis shift signal induced by **18**. Also, the hydroxyl group of IDO1/**24** formed an intramolecular hydrogen bond with the isoindole nitrogen, but in the IDO1/**18** complex structure this cannot take place due to an unfavorable spatial arrangement between the hydroxyl group and the indole nitrogen that precludes the formation of stable five-membered hydrogen bond. In a five-membered hydrogen bonding system, a planar hydrogen bonded conformation with a dihedral angle between the hydrogen bond donor and acceptor of less than 30° is preferred for steric and electrostatic reasons.[33] The dihedral angle between the hydroxyl group (H-bond donor) and the indole nitrogen (H-bond acceptor) of **18** deviates from planarity by 63.8° (Figure 4A) and it is therefore unlikely to form an intramolecular hydrogen bond. In conclusion, the loss of the hydrogen bonding interactions with the heme group, weaker coordinate covalent interactions and the absence of the intramolecular

hydrogen bonding interactions result in the loss of inhibition against IDO1, and shorter red shift in UV-visible spectrum.

Comparison with the Structures of Other Inhibitors Bound to IDO1. The x-ray co-crystal structure of the IDO1/**24** complex was first compared with that of IDO1/4PI[14] (Figure 5A and 5C). 4PI is a fragment-like compound that showed weak inhibition against IDO1 with an IC_{50} value of 48 μM. Superimposing the structures of these two complexes revealed the imidazole ring of 4PI to be located at the sixth coordination site of the heme, and the imidazole nitrogen atom to be covalently bonded to the heme iron. Hydrophobic interactions with Ala264 and Phe163 were also observed. The phenyl ring (ring-2) of 4PI superimposed well with the imidazoleisoindole (ring-3) of **24** and extended to pocket A to form the hydrophobic interactions with Val130, Phe163, Phe164 and Gly262 (Figure 5A). However, in the IDO1/4PI complex structure, 4PI only occupied in the pocket A. In the IDO1/**24** complex structure, however, **24** also directed toward and formed extensive interactions with pocket B. The cyclohexyl group was located in pocket B and made interactions with Phe226, Ile354, Leu384 and Arg231. Furthermore, in the IDO1/4PI complex structure, the propionic acid side chain of the heme was away from the coordinated site and had no interactions with 4PI, whereas in the IDO1/**24** complex structure, the 7- propionic acid of the heme moved toward the coordinated site and

formed a strong hydrogen bond with the hydroxyl group of **24**. Finally, an intramolecular hydrogen bond formed within **24** by the isoindole nitrogen and the hydroxyl group was absent in the IDO1/4PI structure. In conclusion, the additional interactions with pocket B and the extensive hydrogen bonding network with IDO1 are thought to explain the better inhibition of IDO1 by **24** compared with 4PI.

The structure of IDO1/**24** and was also compared with that of IDO1/**27**[15] (Figure 5B and 5C). By superimposing the structure complex of **27** onto **24**, it was found that the *para*-tolyl imidazothiazole moiety (rings 1-3) of **27** occupied a similar position to the imidazoleisoindole core of **24.** Both compounds formed a coordinated covalent bond with the heme iron through the nitrogen atom in the core structures, and made extensive hydrophobic interactions with the surrounding residues in the pocket A. The differences were the hydrogen bond network and the orientation of chloro-phenyl moiety of **27**. The chloro-phenyl moiety of **27** adopted a spatial position different from that of the cyclohexyl moiety of **24.** Compound **27** induced a conformation change by shifting Phe226,[15] and consequently disrupting the edge to face π-π interactions between Phe163 and Phe226. Compound **27** was located next to Phe226 and had no interactions with Arg231. On the other hand, in the structure of IDO1/**24**, Phe226 adopted a conformation similar to that of IDO1/4PI. Compound **24** was positioned between Phe226 and Arg231 and formed the interactions with these two

residues. A mutagenesis study showed that Phe226 and Arg231 play an important role in the catalytic activity of IDO1.[14] Moreover, the hydrogen bond interactions between the **24** and IDO1 are different from that of **27** and IDO1. As described above, extensive hydrogen bond networks were formed by the hydroxyl group of **24**, the 7-propionic acid of the heme, and the main chain NH group of Ala264 and also included an intramolecular hydrogen bond formed within **24**. In the structure of IDO1/**27** complex, the amide group of **27** occupied a similar space to the hydroxyl group of **24** and hence formed the hydrogen bond with the heme, but the 7- propionic acid of the heme formed the hydrogen bond with the side chain of Ser263 instead of the main chain NH group of Ala264. Also, no intramolecular hydrogen bond was observed within **27.** Taken together, these findings explain the decreased activity of **27** compared to **24**.

Stereoisomers of 24. Compound **24** was synthesized as a mixture of four stereoisomers and chiral chromatography was performed by the Daicel Chiral Technologies Co., LTD to separate the mixture (Figure S3 in supporting information). Four peaks were obtained and their inhibitory activities toward IDO1 were evaluated. Peaks 3 and 4 showed potent inhibition of IDO1 with IC_{50} values of 19.5 nM and 28.9 nM, respectively. Peaks 1 and 2 showed weak inhibition to IDO1 with IC_{50} values of 2437 nM and >10000 nM, respectively. These results are consistent with a described

study.[30] In this patent, compounds 1415, 1416, 1417 and 1418 are four stereoisomers and present the same chemical structure as **31**, **30**, **29** and **28**, respectively. The IC_{50} value of compound 1415 (**31)** and compound 1416 (**30)** reported in the patent are 1~ 10 μM while the IC_{50} value of compound 1417 (**29)** and compound 1418 (**28**) are < 1 μM. This data suggests that two stereoisomers, **28** and **29**, significantly contribute to the observed inhibition of IDO1 by **24** (the mixture), whereas the other two stereoisomers, **31** and **30**, do not.

Conclusions

In this study, the structure of IDO1 bound to a potent inhibitor, **24** (a NLG919 analogue), was solved at the resolution of 2.2Å. The density map clearly showed **24** to be located at the sixth coordination site of the heme and covalently bound with the heme iron through the imidazole nitrogen, consistent with the observation by UV-visible spectra that **24** induced a Soret peak shift from 403 to 413 nm. The imidazoleisoindole core was found deep in pocket A, and where it formed extensive hydrophobic interactions with Tyr126, Cys129, Val130, Phe163, Phe164, Gly262, Ala264 and the porphyrin ring. The 1-cyclohexyl ethanol moiety extended to pocket B and formed hydrophobic interactions with Phe226, Ile354 and Leu384. It also had close contacts with Arg231 in the entrance region. Most interestingly, **24** formed an

extensive hydrogen bond network: two intermolecular hydrogen bonds between **24**, the 7- propionic acid of the heme and the main chain NH group of Ala264; and an intramolecular hydrogen bond within **24** by the isoindole nitrogen and the hydroxyl group. This hydrogen bond network is a distinct feature of IDO1/**24** complex structure and is not observed in the other IDO1 complex structures.

Introduction of a fluoro group to the structure of **24** resulted in **25**, which exhibited a 2-fold improvement (IC_{50} = 19 nM) in inhibition of IDO1. Comparison of the IDO1/**25** and IDO1/**24** complex structures revealed that the additional fluorine group of **25** formed an extra halogen bonding interaction with the oxygen atom in the main chain of Gly 262 in pocket A, which could account for the improved potency of **25** compared to **24**.

The role of the hydroxyl group in the binding of IDO1 protein was further investigated by synthesizing compound **23**. Comparison of the structure of IDO1/**23** with that of IDO1/**25** revealed the replacement of hydroxyl group with the carbonyl group resulted in the loss of the intramolecular hydrogen bond, leading to the decreased potency of **23**. The intramolecular hydrogen bond plays a unique role in drug discovery as it could alter the conformation of the molecules[29,34-36] and modulate the physicochemical properties of the designed compounds.[37-39] Studies have shown that intramolecular hydrogen bonds contribute to the improved potency, better cell

permeability, enhanced oral absorption and improved pharmacokinetic properties of compounds.[33,37-41]

Finally, the slight modification of the imidazoleisoindole core of **24** to give **8**, **15**, **18, 20**, **21** and **26** led to a dramatic loss of IDO1 inhibitory activity and also resulted in the shorter Soret band red shift. Further structural biology studies demonstrated that the weaker coordinate covalent interactions and the loss of the hydrogen bonding network completely eliminate the capacity of these analogues to inhibit IDO1.

Novel, small molecular inhibitors of IDO1 are becoming increasingly important due to mounting evidence of the essential role played by IDO1 in cancer immunotherapy. Although a number of IDO1 inhibitors have been identified and developed, only limited structural biology studies of IDO1 inhibitors are available, all of which are weak inhibitors with IC_{50} values in the μM range. The structural biology studies of **24** and its analogues revealed extensive hydrophobic interactions and a unique hydrogen bonding network contributes to the great potency of imidazoleisoindole derivatives. These insights are expected to facilitate the structure-based drug design of new IDO inhibitors.

EXPERIMENTAL Section

General Remarks

Chemicals and solvents were purchased and used as received without further purification. All reactions were carried out under argon atmosphere. Flash column chromatography was performed with Merck Kieselgel 60, No. 9385, 230-400 mesh ASTM silica gel as the stationary phase. Automated flash chromatography was carried out by Teledyne Isco CombiFlash® Automated Flash Chromatography systems. Proton (^{1}H) nuclear magnetic resonance spectra were measured on a Varian Mercury-300 or Varian Mercury-400 spectrometer. Chemical shifts were recorded in parts per million (ppm) on the delta (δ) scale relative to the resonance of the solvent peak. Coupling description was shown by abbreviation: s = singlet; d = doublet; t = triplet; q = quartet; quin = quintet; br = broad; m = multiplet. High-resolution mass spectra (HRMS) were measured by a VARIAN 901-MS electrospray ionization (ESI) or JEOL JMS-700 fast atom bombardment (FAB) mass spectrometer. Purity of the final compounds was determined with an Hitachi 2000 series HPLC system using a C18 column (Agilent ZORBAX Eclipse XDB-C18 5 mm, 4.6 mm × 150 mm), operating at 25 °C. Peaks were detected UV absorption at 254 nm.

4-Iodo-2-methyl-1-trityl-1*H*-imidazole (3). The synthesis of

5-iodo-2-methyl-1*H*-imidazole (**2**) and 4-iodo-2-methyl-1-trityl-1*H*-imidazole (**3**) followed the established procedure with necessary modification.[42] 4-Iodo-2-methyl-1*H*-imidazole (**2**) (3.12 g, 15.0 mmol) in THF (100 mL) was added triethylamine (4.18 mL, 30.0 mmol) and trityl chloride (5.02 g, 18.0 mmol), and then the reaction mixture was reflux for 3 h. After cooling, the suspension was filtered. The filtrate was evaporated in vacuo. The residue was dissolved in dichloromethane (100 mL) and washed with sodium thiosulfate (100 mL, 5% solution in water). The water layer was extracted with dichloromethane (100 mL). The combined organic layer were dried over $MgSO_4$ and concentrated to afford the crude. The crude mixture was purified by automated flash chromatography using 0–4% MeOH : CH_2Cl_2 gradient to give **3** as a pale-yellow solid (3.22 g, 47%). ^{1}H NMR (DMSO-d_6, 400 MHz) δ 7.45–7.39 (m, 9 H), 7.07–7.04 (m, 6 H), 6.65 (s, 1 H), 1.49 (s, 3 H).

2-(2-Methyl-1-trityl-1*H*-imidazol-4-yl)benzaldehyde (5). The synthesis of 2-(2-methyl-1-trityl-1*H*-imidazol-4-yl)benzaldehyde (**5**) followed the established procedure of the NewLink Genetics Corporation, with necessary modifications.[30] A mixture of 4-iodo-2-methyl-1-trityl-1*H*-imidazole (**3**) (1.80 g, 4.00 mmol), 2-foymylphenylboronic acid (**4**) (0.90 g, 6.00 mmol), and potassium phosphate tribasic (2.55 g, 12.0 mmol) in DMF (20 mL) and water (4 mL) was purged with nitrogen for 15 minutes. $Pd(PPh_3)_4$ (0.460 g, 0.400 mmol) was added to the reaction

mixture, and the mixture was purged with nitrogen for another 15 minutes. The reaction mixture was stirred at 90 ^{o}C for 16 h. After cooling, the solution was filtered through a pad of celite. The mixture was diluted with water and extracted with ethyl acetate. The combined organic layer were washed with brine, dried over $MgSO_4$ and concentrated to afford the crude. The crude was purified by automated flash chromatography using 0–6% MeOH : CH_2Cl_2 gradient to give **5** (0.220 g, 13%). ^{1}H NMR ($CDCl_3$, 400 MHz) δ 10.41 (s, 1 H), 7.92 (d, 1 H), 7.74–7.63 (m, 1 H), 7.57 (t, 1 H), 7.41–7.28 (m, 10 H), 7.20–7.16 (m, 6 H), 6.95 (s, 1 H), 1.79 (s, 3 H).

1-Cyclohexyl-2-(3-methyl-5*H*-imidazo[5,1-*a*]isoindol-5-yl)ethanone (7). The synthesis of 1-cyclohexyl-2-(3-methyl-5*H*-imidazo[5,1-*a*]isoindol-5-yl)ethanone (**7**) followed the established procedure of the NewLink Genetics Corporation with necessary modifications.[30] To a solution of 2-(2-methyl-1-trityl-1*H*-imidazol-4-yl)benzaldehyde (**5**) (0.220 g, 0.500 mmol) and cyclohexylmethyl ketone (**6**) (70.0 μL, 0.500 mmol) in THF (3 mL) was added NaOEt (0.20 mL, 0.630 mmol, 21 wt % in ethanol) and the mixture was stirred at room temperature for 3 h. The solvent was concentrated to give the residue, and the residue was diluted with saturated $NH_4Cl_{(aq)}$ (10 mL) and extracted with dichloromethane (2 x 10 mL). The combined organic layer were dried over $MgSO_4$ and concentrated to afford the crude product. The crude was purified by automated flash chromatography

using 0–10% MeOH : CH_2Cl_2 gradient to give **7** as a white solid (75.0 mg, 51%). ^1H NMR ($CDCl_3$, 400 MHz) δ 7.49 (d, 1 H), 7.35 (t, 1 H), 7.27–7.25 (m overlapped with s at 7.26, 1 H), 7.20 (t, 1 H), 7.07 (s, 1 H), 5.72 (dd, 1 H), 3.24 (dd, 1 H), 2.95 (dd, 1 H), 2.47 (s, 3 H), 2.38–2.32 (m, 1 H), 1.95–1.60 (m, 4 H), 1.41–1.18 (m, 6 H).

1-Cyclohexyl-2-(3-methyl-5*H*-imidazo[5,1-*a*]isoindol-5-yl)ethanol (8). The synthesis of 1-cyclohexyl-2-(3-methyl-5*H*-imidazo[5,1-*a*]isoindol-5-yl)ethanol (**8**) followed the established procedure of the NewLink Genetics Corporation with necessary modifications.[30] To a solution of 1-cyclohexyl-2-(3-methyl-5*H*-imidazo[5,1-*a*]isoindol-5-yl)ethanone (**7**) (72.0 mg, 0.240 mmol) in methanol (2 mL) at 0 ^oC was added sodium borohydride (27.8 mg, 0.730 mmol), and the mixture was stirred at room temperature for 2 h. The solvent was removed under reduced pressure and 1N HCl (1 mL) was added to the crude. The solution was stirred for 10 min and was neutralized by saturated. $K_2CO_{3(aq)}$ solution. The aqueous layer was extracted with dichloromethane (2 x 5 mL). The combined organic layer was dried over $MgSO_4$ and concentrated to afford a crude product. the crude was purified by automated flash chromatography using 1–10% MeOH : CH_2Cl_2 gradient to give **8** as a white solid (54.0 mg, 75%). ^1H NMR ($CDCl_3$, 300 MHz) (a mixture of 4 stereoisomers) δ 7.51 (d, 1 H), 7.46 (d, 1 H), 7.36 (t, 1 H), 7.22 (t, 1 H), 7.06 (s, 1 H), 5.40 (dd, 1 H), 3.59–3.51 (m, 1 H), 2.53 (s, 3 H), 2.42–2.27 (m, 1 H),

2.02–1.90 (m, 1 H), 1.72–1.52 (m, 5 H), 1.40–0.88 (m, 6 H). ESMS *m/z* 297.1 (M + 1); HRMS (FAB) *m/z* calcd for $C_{19}H_{24}N_2O$ (M): 296.1889, found 296.1892; HPLC purity of 4 stereoisomers of compound **8** > 99%, t_R = 21.15 min.

2-(1-Trityl-1*H*-imidazol-4-yl)aniline (13). Following the procedure of the synthesis of **5**, a mixture of 4-iodo-1-trityl-1*H*-imidazole (**11**) (1.75 g, 4.00 mmol), 2-aminophenylboronic acid pinacol ester (**12**) (1.31 g, 6.00 mmol), and potassium phosphate tribasic (2.55 g, 12.0 mmol) in DMF (20 mL) and water (4 mL) under nitrogen was added $Pd(PPh_3)_4$ (0.460 g, 0.400 mmol). After work-up, the crude mixture was purified by automated flash chromatography using 0–10% MeOH : CH_2Cl_2 gradient to give the desired product **13** (0.860 g, 53%). ^{1}H NMR ($CDCl_3$, 400 MHz) δ 7.56 (s, 1 H), 7.40–7.34 (m, 9 H), 7.28 (d, 1 H), 7.23–7.18 (m, 6 H), 7.08 (s, 1 H), 7.04 (t, 1 H), 6.73 (d, 1 H), 6.66 (t, 1 H).

1-Cyclohexyl-2-(5,6-dihydroimidazo[1,5-*c*]quinazolin-5-yl)ethanone (14). Following the procedure of the synthesis of **7**, to a solution of 2-(1-trityl-1*H*-imidazol-4-yl)aniline (**13**) (0.270 g, 0.670 mmol) and 3-cyclohexyl-3-oxopropanal (**10**) (0.120 g, 0.800 mmol) in methanol (4 mL) was added acetic acid (1 mL). After work-up, the crude mixture was purified by automated flash chromatography using 3–8% MeOH : CH_2Cl_2 gradient to give **14** as a white solid (100 mg, 51 %). ^{1}H NMR ($CDCl_3$, 400 MHz) δ 7.76 (s, 1 H), 7.48 (d, 1

H), 7.37 (s, 1 H), 7.13 (dd, 1 H), 6.91 (dd, 1 H), 6.76 (d, 1 H), 5.90 (dd, 1 H), 4.94 (br s, 1 H), 3.16–3.05 (m, 2 H), 2.34–2.05 (m overlapped with br s at 2.22, 1 H), 1.90–1.60 (m, 4 H), 1.40–1.19 (m, 6 H).

1-Cyclohexyl-2-(5,6-dihydroimidazo[1,5-*c*]quinazolin-5-yl)ethanol (15). Following the procedure of the synthesis of **8**, 1-cyclohexyl-2-(5,6-dihydroimidazo[1,5-*c*]quinazolin-5-yl)ethanone (**14**) (90.0 mg, 0.300 mmol) was reacted with sodium borohydride (35.0 mg, 0.900 mmol) in methanol (3 mL). After work-up, the crude mixture was purified by automated flash chromatography using 1–8% MeOH : CH_2Cl_2 gradient to give **15** as a white solid (63.0 mg, 69%), which is a mixture of 4 stereoisomers ^{1}H NMR ($CDCl_3$, 400 MHz) (a mixture of 4 stereoisomers) δ 7.85 (s, 1 H), 7.46 (d, 1 H), 7.32 (s, 1 H), 7.11 (t, 1 H), 6.90 (t, 1 H), 6.84–6.70 (m, 1 H), 5.78 (dd, 0.4 H), 5.65 (d, 0.6 H), 3.75–7.63 (m, 0.4 H), 3.46 (dd, 0.6 H), 2.20–1.83 (m, 2 H), 1.83–1.58 (m, 5 H), 1.42–0.83 (m, 6 H). ESMS *m/z* 298.1 (M + 1); HRMS (FAB) *m/z* calcd for $C_{18}H_{23}N_3O$ (M): 297.1841, found 297.1841. HPLC purity of 4 stereoisomers of compound **15** = 92.8%, t_R = 20.63 min.

2-β-Carbolin-9-yl-1-cyclohexyl-ethanol (18). Powdered KOH (126.2 mg, 2.25 mmol) was added to a solution of norharmane (**16**) (252 mg, 1.50 mmol) in anhydrous DMF (1.5 mL) at 0 °C. After stirring at room temperature for 30 min until dissolved,

2-bromo-1-cyclohexylethan-1-one (577 mg, 2.25 mmol) was added *via* syringe and the reaction was stirred at room temperature for 3 h. Upon completion, the solution was partitioned between 30 mL of dichloromethane and 10 mL of water. The aqueous layer was washed with dichloromethane (3 x 30 mL), and the combined organics were washed with brine, dried over Na_2SO_4, filtered, and concentrated under reduced pressure. The residue was purified by column chromatography (MeOH : CH_2Cl_2) to afford ketone **17** (156 mg, 36%). To a solution of ketone **17** (143 mg, 0.489 mmol) in MeOH (5.0 mL) was added sodium borohydride (17.4 mg, 0.978 mmol) at 0 °C. After stirring at the same temperature for 30 min, the reaction mixture was quenched by water and concentrated under reduced pressure. The residue was partitioned between 30 mL of dichloromethane and 10 mL of water, the aqueous layer was washed dichloromethane (3 x 30 mL), and the combined organics were washed with brine, dried over Na_2SO_4, filtered, and concentrated under reduced pressure. The residue was purified by column chromatography (MeOH : CH_2Cl_2) to afford **18** as a yellow solid (128 mg, 89%). ^{1}H NMR (400 MHz, $CDCl_3$) δ 8.79 (s, 1H), 8.25 (d, 1H), 8.10 (d, 1H), 7.83 (d, 1H), 7.59 (td, 1H), 7.51 (d, 1H), 7.28 (td, 1H), 4.43 (dd, 1H), 4.33 (dd, 1H), 3.94–3.89 (m, 1H), 2.05–2.02 (m, 1H), 1.91–1.85 (m, 2H), 1.76–1.73 (m, 1H), 1.64–1.60 (m, 1H), 1.37–1.19 (m, 5H); ESMS *m/z*: 295.1 (M + 1); HRMS (ESI) *m/z* calcd for $C_{19}H_{23}N_2O$ (M+1):295.1810, found 295.1804; HPLC purity = 98.7 %. t_R

= 22.99 min.

1-Cyclohexyl-2-pyrido[2,3-*b*]indol-9-yl-ethanone (20). The synthesis of 1-cyclohexyl-2-pyrido[2,3-*b*]indol-9-yl-ethanone (**20**) followed the procedure for preparation of **17**. Powdered KOH (23.0 mg, 0.414 mmol) was added to a solution of α-carboline (46.5 mg, 0.276 mmol) in anhydrous DMF (1.0 mL), then reacted with 2-bromo-1-cyclohexylethan-1-one (90.0 mg, 0.414 mmol). After work-up, the residue was purified by column chromatography (ethyl acetate: hexane = 1:1) to afford **20** as yellow oil (35.7 mg, 44%). ^{1}H NMR (400 MHz, $CDCl_3$) δ 8.44 (dd, 1H), 8.32 (dd, 1H), 8.08 (d, 1H), 7.48 (td, 1H), 7.28 (td, 1H), 7.21–7.17 (m, 2H), 5.30 (s, 2H), 2.56 (tt, 1H), 1.99–1.95 (m, 2H), 1.82–1.78 (m, 2H), 1.67–1.65 (m, 1H), 1.46–1.41 (m, 2H), 1.29–1.20 (m, 3H); ESMS *m/z*: 293.1 (M + 1); HRMS (ESI) *m/z* calcd for $C_{19}H_{23}N_2O$ (M+1): 293.1654, found 293.1648; HPLC purity = 99 %, t_R = 43.34 min.

1-Cyclohexyl-2-pyrido[2,3-*b*]indol-9-yl-ethanol (21). The synthesis of 1-cyclohexyl-2-pyrido[2,3-*b*]indol-9-yl-ethanol (**21**) followed the procedure for preparation of **18**. To a solution of 1-cyclohexyl-2-pyrido[2,3-*b*]indol-9-yl-ethanone (**20**) (23.3 mg, 0.08 mmol) in MeOH (1.5 mL) was added sodium borohydride (6.00 mg, 0.160 mmol). After work-up, the residue was purified by column chromatography (ethyl acetate : hexane = 1:1) to afford **21** as a yellow solid (16.1 mg, 68%). ^{1}H NMR

(400 MHz, $CDCl_3$) δ 8.43 (dd, 1H), 8.34 (dd, 1H), 8.08 (dt, 1H), 7.53 (d, 1H), 7.29 (td, 1H), 7.18 (dd, 1H), 4.89 (s, 1H), 4.52–4.49 (m, 2H), 3.88–3.84 (m, 1H), 2.03–2.01 (m, 1H), 1.90–1.57 (m, 7H), 1.32–1.19 (m, 3H); ESMS *m/z*: 295.1 (M + 1). HRMS (ESI) *m/z* calcd for $C_{19}H_{23}N_2O$ (M+1):295.1810, found 295.1807; HPLC purity = 99 %. t_R = 42.08 min.

Enzyme-based IDO activity assay. The enzymatic inhibition assays were performed as previous described.[43] Briefly, 10 μL IDO1 enzyme (25 μg/mL) was added to 90 μL standard assay medium [50 mM potassium phosphate buffer (pH 6.5), 10 mM ascorbic acid (neutralized with 1M NaOH solution), 10 μM methylene blue, 100 μg/mL catalase, 200 μM L-tryptophan] in 96-well black plate. Followed the 10 μL tested compounds (100 μM in potassium phosphate buffer) were added to 96-well plate and mixed 3 times. The reaction was carried out at 37 ℃ for 1 hr. To convert *N*-formylkynurenine to kynurenine, 20 μL NaOH (1M) was added and incubated at 60 ℃ for 4 hr. Cooled the mixture at 4 ℃ for 10 min and centrifuged at 800*g* for 3 min at room temperature. The amount of kynurenine production from reaction was measured by the emission of fluorescence at 460 nm using a Victor 2 multilabel reader (PerkinElmer Inc.). The inhibition percentage was determined as [100-(A/B)x100]/100, where A was the IDO1 activity with test compound added to protein and B was the absence of test compound.

Cell-based assay. HeLa cells were seeded in 96-well culture plates at a density of $1x10^4$ per well. On the next day, human IFN-γ (10 ng/mL) and compounds in a total volume of 200 μL culture medium containing 15 μg/mL of L-tryptophan were added to the cells. After incubation for 24 hours, 140 μL of the supernatant was mixed with 10 μL of 6.1N trichloroacetic acid and the mixture was incubated for 30 min at 50°C. The reaction mixture was then centrifuged for 10 minutes at 2500 rpm to remove sediments. 100 μL of the supernatant was mixed with 100μL of 2% (w/v) p-dimethylaminobenzaldehyde in acetic acid and measured at 480 nm.

UV-Visible spectra. UV-Visible scan (200-700 nm) were performed and recorded on NanoDrop 2000 (Thermo Fisher Scientific Inc.) with 300 μM IDO1 mixed with 2 mM of tested compounds.

Protein expression and purification of recombinant human IDO1. The human IDO1 was cloned into pET14b (Novagen) and over-expressed in bacterial strain BL21(DE3). The cells were harvested and frozen at -80°C for further purification. The cell pellets were suspended in buffer solution containing 25 mM Tris-Cl, 500 mM NaCl, 10 mM $MgCl_2$, pH 7.4, and lysed by sonication. Cell extracts were followed by loading to Nicole column (GE Healthcare) and washed. The eluted protein was exchanged to thrombin cleavage buffer and digested by thrombin protease. The his-tag was removed by loading the digested mixture to desalting column. The

flow-through was then buffer exchanged to final buffer (25 mM 2-(*N*-morpholino)ethanesulfonic acid (MES), 25 mM NaCl, pH 6.5) and concentrated to 30 mg/mL.

Protein crystallography and Data collection. The purified human IDO protein was mixed with compounds, and co-crystallized by hanging drop vapor diffusion method. The co-crystals were grown at 18°C for 1-2 weeks in reservoir solution containing 2-18 % polyethylene glycol, and 0.2 M Ammonium salt. The crystals were cryoprotected by soaking in the reservoir with glycerol. Diffraction data set were collected at the NSRRC (beamline BL13B1 and BL13C1) and SPring8 synchrotron facility (beamline 44XU). The structures were solved by the molecular replacement method MOLREP[44] of the CCP4 program suites[45] using the IDO1 structures (PDB code: 2D0T) as a search model. The structures were refined by utilizing REFMAC[46] followed by model building with program O[47], and PHENIX[48]. The completed structure model was optimized by using a PDB_REDO.[49] The final models were validated using Molprobity.[50] All structural figures were generated using PyMOL (Schrödinger, USA).

Figure 1. UV spectra of ferric IDO1 without (blue) and with 2 mM concentration of compound **24** (red). In the presence of **24**, the Soret peak shifts from 403 to 413 nm.

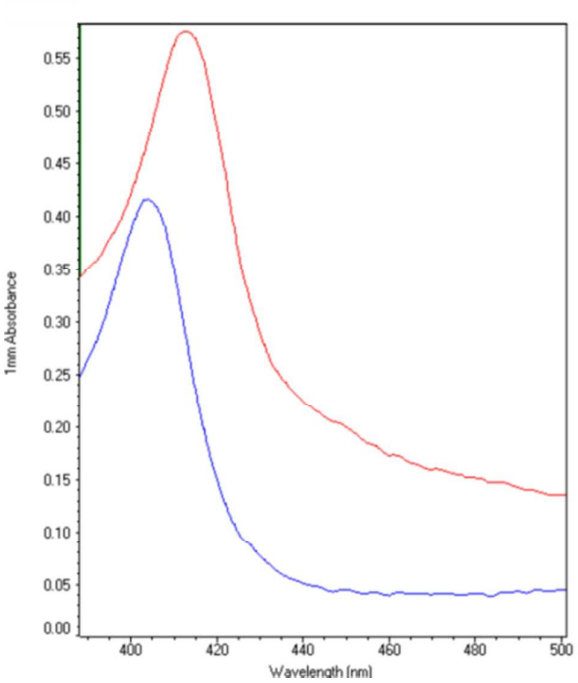

Figure 2. (A) Crystal structure of IDO1/**24**. The red dashed lines indicate hydrogen bonds (B) The hydrogen bond network of **24** in IDO1.

(A)

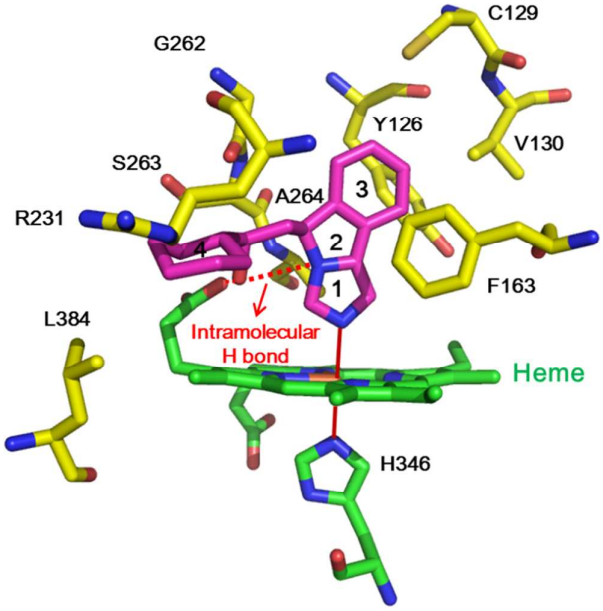

(B)

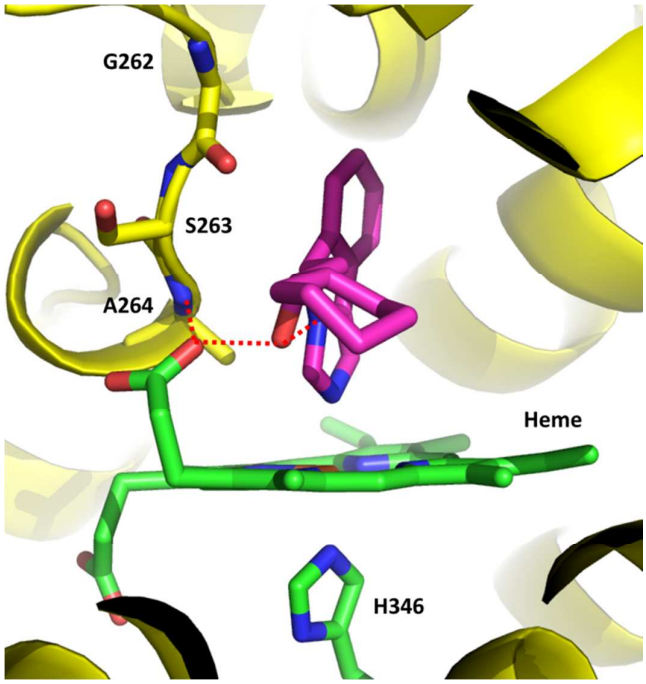

Figure 3. (A) Crystal structure of IDO1/**25** (magenta) (B) Crystal structure of IDO1/**23** (light blue) and (C) Superimposition of **23**, **25**, and **24** (yellow) in IDO1. The red dashed lines indicate hydrogen bonds; the green dashed line indicates a halogen bond.

(A)

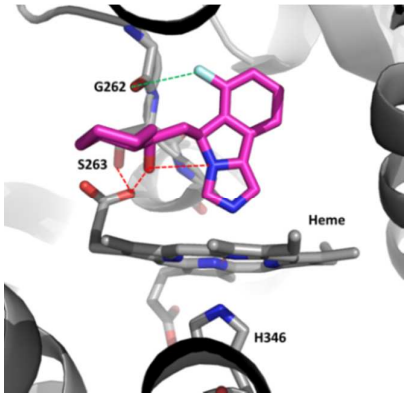

(B)

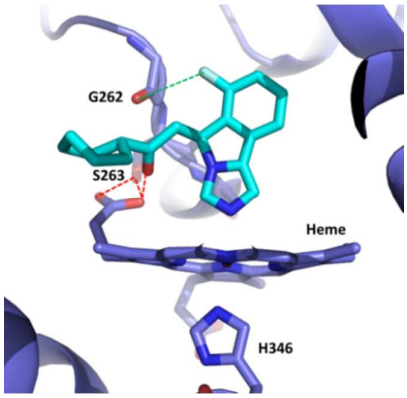

(C)

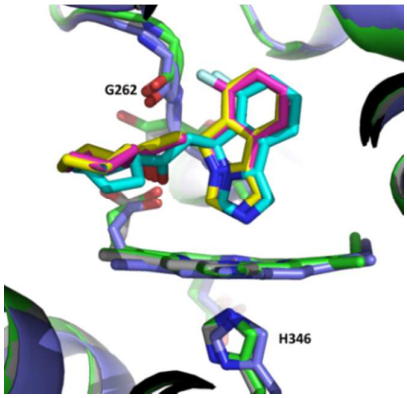

Figure 4. (A) Crystal structures of IDO1 (purple) /**18** (pale pink) complex. An unfavorable dihedral angle (-63.8°) between the indole nitrogen and hydroxyl group in **18** precludes the formation of an intramolecular hydrogen bond. (B) Superimposition of **18** (pale pink) and **24** (yellow) in IDO1.

(A)

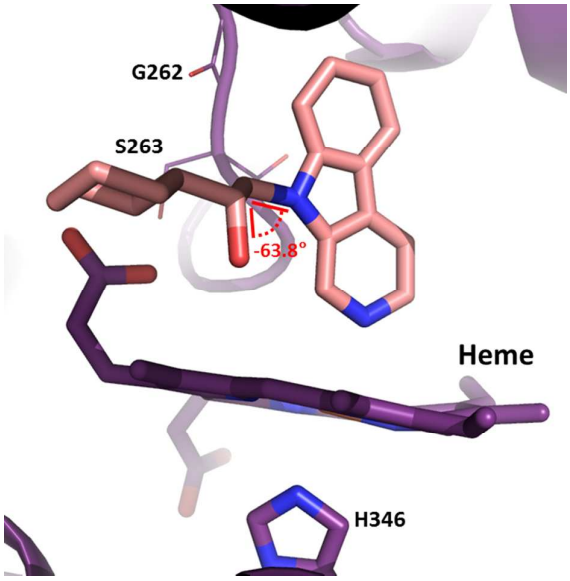

(B)

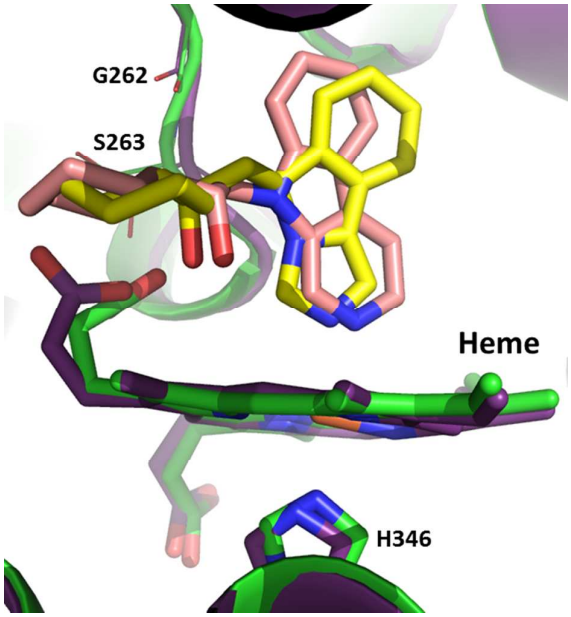

Figure 5. (A) Comparison of the structures of IDO1/**24** (yellow) and IDO1/4PI (magenta). (B) Comparison of the structures of IDO1/**24** (yellow) and IDO1/**27** (purple) complex structure. (C) Chemical structures of **24**, **27** and 4PI. For comparison, the rings of compound structures are labeled.

(A)

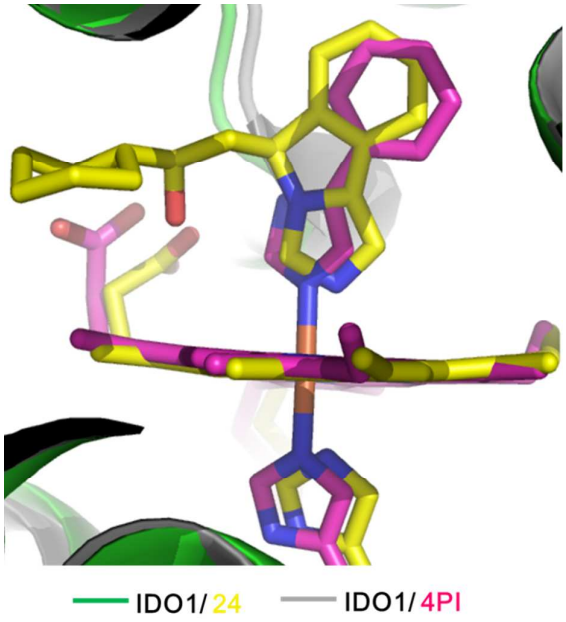

(B)

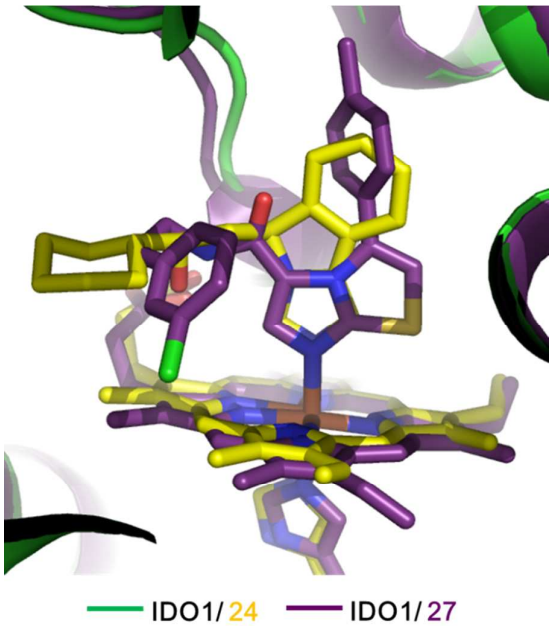

(C)

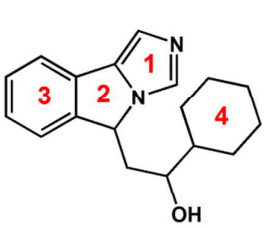

24

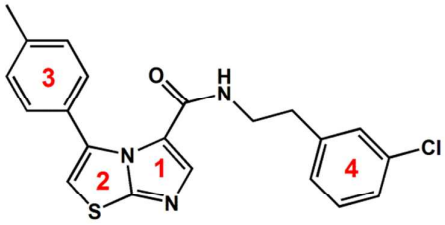

27

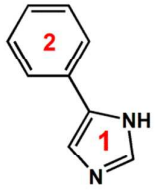

4PI

Scheme 1.

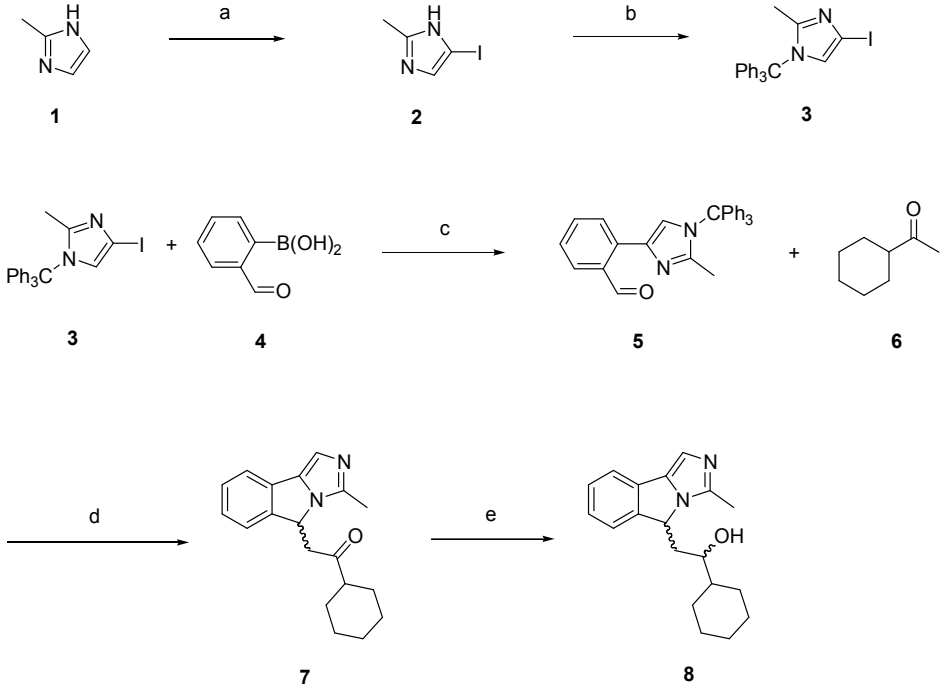

Reagents and conditions: Reagents and conditions: (a) 1. KI, I_2, NaOH, H_2O, 16 h, rt; 2. AcOH, rt; 3. Na_2SO_3, EtOH, 36 h, reflux. (91 %) (b) Ph_3CCl, Et_3N, THF, 3 h, reflux. (47 %) (c) K_3PO_4, $Pd(PPh_3)_4$, DMF/H_2O, 16 h, 90 °C. (13 %) (d) 1. NaOEt, THF, 3 h, rt; 2. AcOH, MeOH, 16 h, 90 °C. (51 %) (e) $NaBH_4$, MeOH, 2 h, rt. (75 %)

Scheme 2.

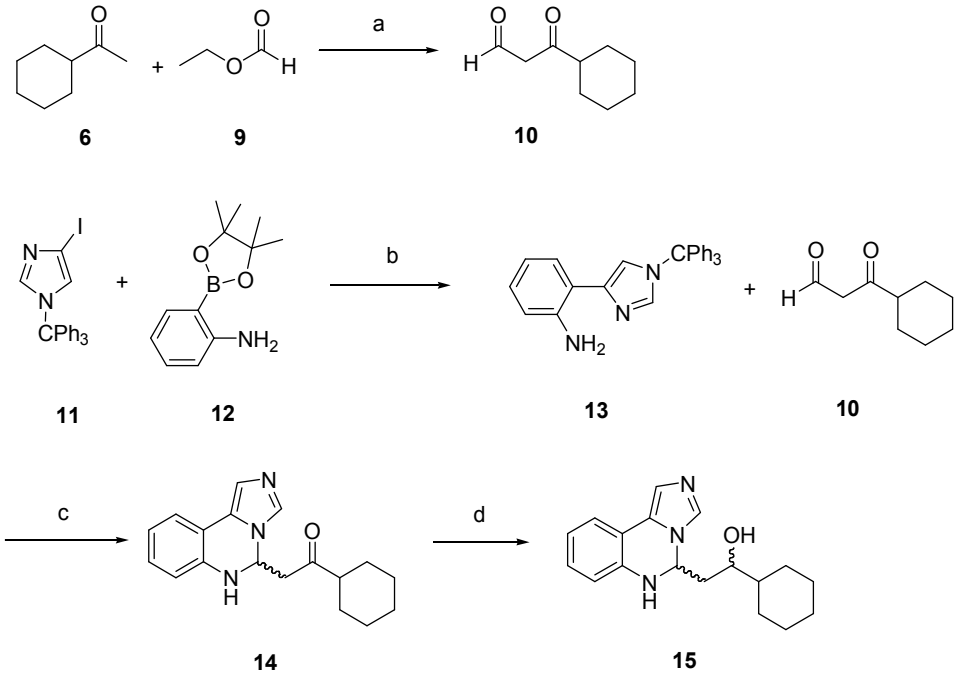

6 9 10 11 12 13 10 14 15

Reagents and conditions: (a) NaH, *t*-BuOMe, (b) K_3PO_4, $Pd(PPh_3)_4$, DMF/H_2O, 16 h, 90 °C. (53 %) (c) AcOH, MeOH, 16 h, 90 °C. (51 %) (d) $NaBH_4$, MeOH, 2 h, rt. (69 %)

Scheme 3.

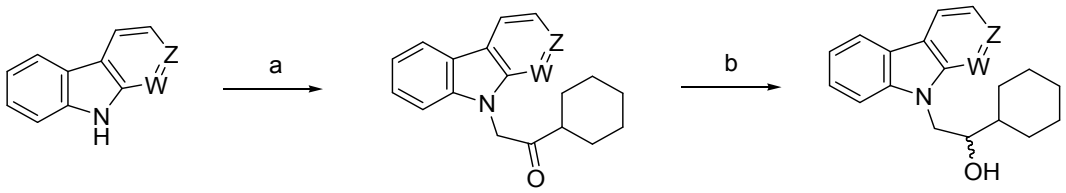

16 W = C, Z = N
19 W = N, Z = C

17 W = C, Z = N
20 W = N, Z = C

18 W = C, Z = N
21 W = N, Z = C

Reagents and conditions: (a) 2-Bromo-1-cyclohexylethan-1-one, KOH, DMF, 3 h, rt. (36–44 %) (b) $NaBH_4$, MeOH, 0.5 h, 0 °C. (68–89 %)

Table 1. Enzymatic and cellular assay for IDO inhibition.

Compound		Enzymatic assay[a] IC_{50} (nM) hIDO	Cellular assay[a] EC_{50} (nM) HeLa (IDO)	UV-Vis scan (nm)
22	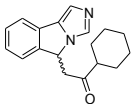	468	749	403-->413
23	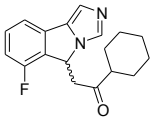	279	725	403-->413
24	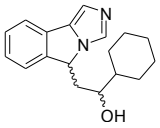	38	61	403-->413
25	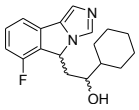	19	55	403-->413
8	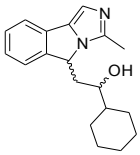	>10,000	>10,000	403-->405
26	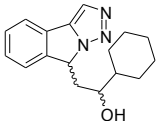	>10,000	>10,000	403-->413
15	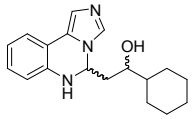	1139	>10,000	403-->413
18	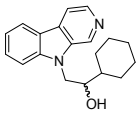	>10,000	ND	403-->407
20	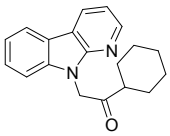	>10,000	ND	403-->403
21	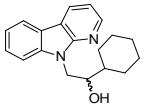	>10,000	ND	403-->403

ND = Not determined.

[a] Values are expressed as the mean of at least three independent determinations and are within ±15%

ASSOCIATED CONTENT

Supporting Information

The density map of the structure of IDO1/**24**, molecular docking study of **15,** chiral chromatography results, data collection and refinement statistics for X-ray crystallography, Chemical syntheses of compounds **22**-**26**, Analytical data (HPLC traces) of compounds **8**, **15**, **18, 20**, **21, 22**, **23**, **24**, **25** and **26**. This material is available free of charge via the Internet at http://pubs.acs.org.

PDB ID Codes: 5EK2, 5EK3, 5EK4

AUTHOR INFORMATION

Corresponding Author

* Phone: +886-37-246-166 extension 35713. Fax: + 886-37-586-456. Email: suying@nhri.org.tw for SYW ;

Funding Sources

Grants supports were from National Health Research Institute, Taiwan, ROC (BP-103-PP-04), National Science Council (Grant No. NSC-102-2325-B-400-001 for Dr. SYW) and Ministry of Health and Welfare (Grant No. MOHW103-TDU-212-114006)

ACKNOWLEDGMENT

We thank the staff of beamline BL13B1 and BL13C1 at the National Synchrotron Radiation Research Center (NSRRC), Taiwan, and 44XU and SP12B2 at Spring-8, Japan, for technical assistance.

ABBREVIATIONS

IDO1, Indoleamine 2,3-Dioxygenase 1; TAAs, tumor associated antigens; 4PI, 4-phenylimidazole; SAR, structure-activity relationships.

Reference

(1) Lob, S.; Konigsrainer, A.; Rammensee, H. G.; Opelz, G.; Terness, P. Inhibitors of indoleamine-2,3-dioxygenase for cancer therapy: can we see the wood for the trees? *Nat. Rev. Cancer* **2009,** *9*, 445-452.

(2) Munn, D. H.; Mellor, A. L. Indoleamine 2,3-dioxygenase and tumor-induced tolerance. *J. Clin. Invest.* **2007,** *117*, 1147-1154.

(3) Hwu, P.; Du, M. X.; Lapointe, R.; Do, M.; Taylor, M. W.; Young, H. A. Indoleamine 2,3-dioxygenase production by human dendritic cells results in the inhibition of T cell proliferation. *J. Immunol.* **2000,** *164*, 3596-3599.

(4) Curti, A.; Trabanelli, S.; Salvestrini, V.; Baccarani, M.; Lemoli, R. M. The role of indoleamine 2,3-dioxygenase in the induction of immune tolerance: focus on hematology. *Blood* **2009,** *113*, 2394-2401.

(5) Smith, C.; Chang, M. Y.; Parker, K. H.; Beury, D. W.; DuHadaway, J. B.; Flick, H. E.; Boulden, J.; Sutanto-Ward, E.; Soler, A. P.; Laury-Kleintop, L. D.; Mandik-Nayak, L.; Metz, R.; Ostrand-Rosenberg, S.; Prendergast, G. C.; Muller, A. J. IDO is a nodal pathogenic driver of lung cancer and metastasis development. *Cancer Discov.* **2012,** *2*, 722-735.

(6) Yue, E. W.; Douty, B.; Wayland, B.; Bower, M.; Liu, X.; Leffet, L.; Wang, Q.;

Bowman, K. J.; Hansbury, M. J.; Liu, C.; Wei, M.; Li, Y.; Wynn, R.; Burn, T. C.; Koblish, H. K.; Fridman, J. S.; Metcalf, B.; Scherle, P. A.; Combs, A. P. Discovery of potent competitive inhibitors of indoleamine 2,3-dioxygenase with in vivo pharmacodynamic activity and efficacy in a mouse melanoma model. *J. Med. Chem.* **2009,** *52*, 7364-7367.

(7) Koblish, H. K.; Hansbury, M. J.; Bowman, K. J.; Yang, G.; Neilan, C. L.; Haley, P. J.; Burn, T. C.; Waeltz, P.; Sparks, R. B.; Yue, E. W.; Combs, A. P.; Scherle, P. A.; Vaddi, K.; Fridman, J. S. Hydroxyamidine inhibitors of indoleamine-2,3-dioxygenase potently suppress systemic tryptophan catabolism and the growth of IDO-expressing tumors. *Mol. Cancer Ther.* **2010,** *9*, 489-498.

(8) Mario R. Mautino, F. A. J., Jesse Waldo, Sanjeev Kumar, James Adams, Clarissa Van Allen, Agnieszka Marcinowicz-Flick, David Munn, Nicholas Vahanian, Charles J. . NLG919, a novel indoleamine-2,3-dioxygenase (IDO)-pathway inhibitor drug candidate for cancer therapy. *AACR* **2013,** *Abstract number 491*.

(9) Rohrig, U. F.; Majjigapu, S. R.; Vogel, P.; Zoete, V.; Michielin, O. Challenges in the Discovery of Indoleamine 2,3-Dioxygenase 1 (IDO1) Inhibitors. *J. Med. Chem.* **2015**.

(10) Meininger, D.; Zalameda, L.; Liu, Y.; Stepan, L. P.; Borges, L.; McCarter, J. D.; Sutherland, C. L. Purification and kinetic characterization of human indoleamine

2,3-dioxygenases 1 and 2 (IDO1 and IDO2) and discovery of selective IDO1 inhibitors. *Biochim. Biophys. Acta.* **2011,** *1814*, 1947-1954.

(11) Balog, J. H., A.; Chen, B.; Chen, L.; Shan, W. IDO inhibitors. *Patent WO2014/150646,* **2014**.

(12) Sheridan, C. IDO inhibitors move center stage in immuno-oncology. *Nat. Biotechnol.* **2015,** *33*, 321-322.

(13) Banerjee, M. M., S.; Shrivastava, R.; Raina, S.; Surya, A.; Yadav, V. K.; Kapoor, K. K. Aminonitriles as kynurenine pathway inhibitors. *Patent WO2014/141110,* **2014**.

(14) Sugimoto, H.; Oda, S.; Otsuki, T.; Hino, T.; Yoshida, T.; Shiro, Y. Crystal structure of human indoleamine 2,3-dioxygenase: catalytic mechanism of O2 incorporation by a heme-containing dioxygenase. *Proc. Natl. Acad. Sci. U. S. A.* **2006,** *103*, 2611-2616.

(15) Tojo, S.; Kohno, T.; Tanaka, T.; Kamioka, S.; Ota, Y.; Ishii, T.; Kamimoto, K.; Asano, S.; Isobe, Y. Crystal Structures and Structure-Activity Relationships of Imidazothiazole Derivatives as IDO1 Inhibitors. *ACS Med. Chem. Lett.* **2014,** *5*, 1119-1123.

(16) Sono, M.; Cady, S. G. Enzyme kinetic and spectroscopic studies of inhibitor and effector interactions with indoleamine 2,3-dioxygenase. 1. Norharman and 4-phenylimidazole binding to the enzyme as inhibitors and heme ligands.

Biochemistry **1989,** *28*, 5392-5399.

(17) Kumar, S.; Jaller, D.; Patel, B.; LaLonde, J. M.; DuHadaway, J. B.; Malachowski, W. P.; Prendergast, G. C.; Muller, A. J. Structure based development of phenylimidazole-derived inhibitors of indoleamine 2,3-dioxygenase. *J. Med. Chem.* **2008,** *51*, 4968-4977.

(18) Dounay, A. B.; Tuttle, J. B.; Verhoest, P. R. Challenges and Opportunities in the Discovery of New Therapeutics Targeting the Kynurenine Pathway. *J Med Chem* **2015**, [Online early access]. DOI:10.1021/acs.jmedchem.1025b00461. Published online: July 24, 2015.

(19) Dawson, J. H.; Andersson, L. A.; Sono, M. Spectroscopic investigations of ferric cytochrome P-450-CAM ligand complexes. Identification of the ligand trans to cysteinate in the native enzyme. *J. Biol. Chem.* **1982,** *257*, 3606-3617.

(20) Littlejohn, T. K.; Takikawa, O.; Skylas, D.; Jamie, J. F.; Walker, M. J.; Truscott, R. J. Expression and purification of recombinant human indoleamine 2, 3-dioxygenase. *Protein Expr. Purif.* **2000,** *19*, 22-29.

(21) Rohrig, U. F.; Majjigapu, S. R.; Grosdidier, A.; Bron, S.; Stroobant, V.; Pilotte, L.; Colau, D.; Vogel, P.; Van den Eynde, B. J.; Zoete, V.; Michielin, O. Rational design of 4-aryl-1,2,3-triazoles for indoleamine 2,3-dioxygenase 1 inhibition. *J. Med. Chem.* **2012,** *55*, 5270-5290.

(22) Schenkman, J. B.; Sligar, S. G.; Cinti, D. L. Substrate interaction with cytochrome P-450. *Pharmacol. Ther.* **1981,** *12*, 43-71.

(23) Brown, D. G.; Flocco, M. M. Useful crystallographic terminology when utilising crystal structures. In *Structure-based drug discovery: an overview*, Hubbard, R. E., Ed. Royal Society of Chemistry: UK, 2006; p 38.

(24) Wlodawer, A.; Minor, W.; Dauter, Z.; Jaskolski, M. Protein crystallography for aspiring crystallographers or how to avoid pitfalls and traps in macromolecular structure determination. *FEBS J.* **2013,** *280*, 5705-5736.

(25) Smart, O. S.; Bricogne, G. Achieving High Quality Ligand Chemistry in Protein-Ligand Crystal Structures for Drug Design. In *Multifaceted Roles of Crystallography in Modern Drug Discovery*, Scapin, G.; Patel, D.; Arnold, E., Eds. Springer Netherlands: UK, 2015; pp 165-181.

(26) Smart, O. S.; Womack, T. O.; Flensburg, C.; Keller, P.; Paciorek, W.; Sharff, A.; Vonrhein, C.; Bricogne, G. Exploiting structure similarity in refinement: automated NCS and target-structure restraints in BUSTER. *Acta. Crystallogr. D Biol. Crystallogr.* **2012,** *68*, 368-380.

(27) Das, A.; Zhao, J.; Schatz, G. C.; Sligar, S. G.; Van Duyne, R. P. Screening of type I and II drug binding to human cytochrome P450-3A4 in nanodiscs by localized surface plasmon resonance spectroscopy. *Anal. Chem.* **2009,** *81*, 3754-3759.

(28) Martin, S. F. Preorganization in biological systems: Are conformational constraints worth the energy? *Pure Appl. Chem.* **2007,** *79*, 193-200.

(29) Harter, W. G.; Albrect, H.; Brady, K.; Caprathe, B.; Dunbar, J.; Gilmore, J.; Hays, S.; Kostlan, C. R.; Lunney, B.; Walker, N. The design and synthesis of sulfonamides as caspase-1 inhibitors. *Bioorg. Med. Chem. Lett.* **2004,** *14*, 809-812.

(30) Mautino, M., Kumar, S., Waldo, J., Jaipuri, F., Kesharwani, T., Zhang, X. Fused imidazole derivatives useful as IDO inhibitors. *Patent WO 2012/142237,* **2012**.

(31) Hintermann, L.; Dang, T. T.; Labonne, A.; Kribber, T.; Xiao, L.; Naumov, P. The AZARYPHOS family of ligands for ambifunctional catalysis: syntheses and use in ruthenium-catalyzed anti-Markovnikov hydration of terminal alkynes. *Chem. Eur. J.* **2009,** *15*, 7167-7179.

(32) Kumar, S., Waldo, J., Jaipuri, F., Mautino, M. Tricyclic compounds as inhibitors of immunosuppression mediated by tryptophan metabolization. *Patent WO2014/159248,* **2014**.

(33) Kuhn, B.; Mohr, P.; Stahl, M. Intramolecular hydrogen bonding in medicinal chemistry. *J. Med. Chem.* **2010,** *53*, 2601-2611.

(34) Nomura, M.; Kinoshita, S.; Satoh, H.; Maeda, T.; Murakami, K.; Tsunoda, M.; Miyachi, H.; Awano, K. (3-substituted benzyl)thiazolidine-2,4-diones as structurally new antihyperglycemic agents. *Bioorg. Med. Chem. Lett.* **1999,** *9*, 533-538.

(35) Van Zandt, M. C.; Sibley, E. O.; McCann, E. E.; Combs, K. J.; Flam, B.; Sawicki, D. R.; Sabetta, A.; Carrington, A.; Sredy, J.; Howard, E.; Mitschler, A.; Podjarny, A. D. Design and synthesis of highly potent and selective (2-arylcarbamoyl-phenoxy)-acetic acid inhibitors of aldose reductase for treatment of chronic diabetic complications. *Bioorg. Med. Chem.* **2004,** *12*, 5661-5675.

(36) Furet, P.; Bold, G.; Hofmann, F.; Manley, P.; Meyer, T.; Altmann, K. H. Identification of a new chemical class of potent angiogenesis inhibitors based on conformational considerations and database searching. *Bioorg. Med. Chem. Lett.* **2003,** *13*, 2967-2971.

(37) Ashwood, V. A.; Field, M. J.; Horwell, D. C.; Julien-Larose, C.; Lewthwaite, R. A.; McCleary, S.; Pritchard, M. C.; Raphy, J.; Singh, L. Utilization of an intramolecular hydrogen bond to increase the CNS penetration of an NK(1) receptor antagonist. *J. Med. Chem.* **2001,** *44*, 2276-2285.

(38) Sasaki, S.; Cho, N.; Nara, Y.; Harada, M.; Endo, S.; Suzuki, N.; Furuya, S.; Fujino, M. Discovery of a thieno[2,3-d]pyrimidine-2,4-dione bearing a p-methoxyureidophenyl moiety at the 6-position: a highly potent and orally bioavailable non-peptide antagonist for the human luteinizing hormone-releasing hormone receptor. *J. Med. Chem.* **2003,** *46*, 113-124.

(39) Rezai, T.; Bock, J. E.; Zhou, M. V.; Kalyanaraman, C.; Lokey, R. S.; Jacobson,

M. P. Conformational flexibility, internal hydrogen bonding, and passive membrane permeability: successful in silico prediction of the relative permeabilities of cyclic peptides. *J. Am. Chem. Soc.* **2006,** *128*, 14073-14080.

(40) Over, B.; McCarren, P.; Artursson, P.; Foley, M.; Giordanetto, F.; Gronberg, G.; Hilgendorf, C.; Lee, M. D. t.; Matsson, P.; Muncipinto, G.; Pellisson, M.; Perry, M. W.; Svensson, R.; Duvall, J. R.; Kihlberg, J. Impact of stereospecific intramolecular hydrogen bonding on cell permeability and physicochemical properties. *J. Med. Chem.* **2014,** *57*, 2746-2754.

(41) Abraham, M. H.; Ibrahim, A.; Zissimos, A. M.; Zhao, Y. H.; Comer, J.; Reynolds, D. P. Application of hydrogen bonding calculations in property based drug design. *Drug Discov. Today* **2002,** *7*, 1056-1063.

(42) Wijtmans, M.; Celanire, S.; Snip, E.; Gillard, M. R.; Gelens, E.; Collart, P. P.; Venhuis, B. J.; Christophe, B.; Hulscher, S.; van der Goot, H.; Lebon, F.; Timmerman, H.; Bakker, R. A.; Lallemand, B. I.; Leurs, R.; Talaga, P. E.; de Esch, I. J. 4-benzyl-1H-imidazoles with oxazoline termini as histamine H3 receptor agonists. *J. Med. Chem.* **2008,** *51*, 2944-2953.

(43) Cheng, M. F.; Hung, M. S.; Song, J. S.; Lin, S. Y.; Liao, F. Y.; Wu, M. H.; Hsiao, W.; Hsieh, C. L.; Wu, J. S.; Chao, Y. S.; Shih, C.; Wu, S. Y.; Ueng, S. H. Discovery and structure-activity relationships of phenyl benzenesulfonylhydrazides as novel

indoleamine 2,3-dioxygenase inhibitors. *Bioorg. Med. Chem. Lett.* **2014,** *24*, 3403-3406.

(44) Vagin, A.; Teplyakov, A. MOLREP: an automated program for molecular replacement. *J. Appl. Crystallogr.* **1997,** *30*, 1022 -1025.

(45) Bailey, S. The CCP4 suite: programs for protein crystallography. *Acta. Crystallogr. D Biol. Crystallogr.* **1994,** *50*, 760-763.

(46) Murshudov, G. N.; Vagin, A. A.; Dodson, E. J. Refinement of macromolecular structures by the maximum-likelihood method. *Acta. Crystallogr. D Biol. Crystallogr.* **1997,** *53*, 240-255.

(47) Jones, T. A.; Zou, J. Y.; Cowan, S. W.; Kjeldgaard, M. Improved methods for building protein models in electron density maps and the location of errors in these models. *Acta. Crystallogr. A* **1991,** *47*, 110-119.

(48) Afonine, P. V.; Grosse-Kunstleve, R. W.; Echols, N.; Headd, J. J.; Moriarty, N. W.; Mustyakimov, M.; Terwilliger, T. C.; Urzhumtsev, A.; Zwart, P. H.; Adams, P. D. Towards automated crystallographic structure refinement with phenix.refine. *Acta. Crystallogr. D Biol. Crystallogr.* **2012,** *68*, 352-367.

(49) R. P. Joosten; J. Salzemann; V. Bloch; H. Stockinger; A.-C. Berglund; C. Blanchet; E. Bongcam-Rudloff; C. Combet; A. L. Da Costa; G. Deleage; M. Diarena; R. Fabbretti; G. Fettahi; V. Flegel; A. Gisel; V. Kasam; T. Kervinen; E. Korpelainen;

K. Mattila; M. Pagni; M. Reichstadt; V. Breton; I. J. Tickle; Vriend, G. PDB_REDO: automated re-refinement of X-ray structure models in the PDB. *J. Appl. Crystallogr.* **2009,** *42*, 376-384.

(50) Chen, V. B.; Arendall, W. B., 3rd; Headd, J. J.; Keedy, D. A.; Immormino, R. M.; Kapral, G. J.; Murray, L. W.; Richardson, J. S.; Richardson, D. C. MolProbity: all-atom structure validation for macromolecular crystallography. *Acta. Crystallogr. D Biol. Crystallogr.* **2010,** *66*, 12-21.

Table of Contents Graphic

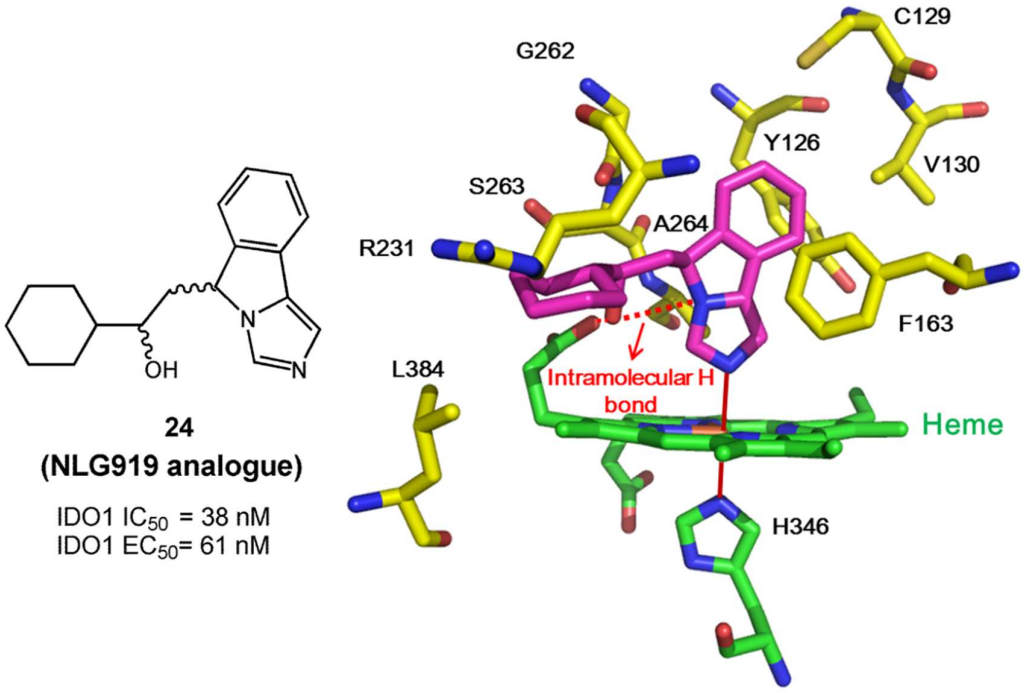

24
(NLG919 analogue)

IDO1 IC_{50} = 38 nM
IDO1 EC_{50}= 61 nM